Basic physical properties of sediment cores collected in the Chilean marginal area and Magellan Strait during leg.3 of cruise MR03-K04.

Naomi Harada¹, Naokazu Ahagon^{1, 2}, Carina B. Lange³, Yoshihiro Asahara⁴, Silvio Pantoja³, Margarita E. Marchant³, Toshiaki Mishima⁵, Hirohide Kanke^{1, 4}, Raul I. Tapia³, Julio Sepulueda³, Aljandro J.A. Santis³, Kota Katsuki⁶, Yutaka Matsuura⁷, Yuusuke Sato⁷, Rena Maeda⁷, Tamami Ueno⁷, Wataru Tokunaga⁸, Ryo Kimura⁸ and Norio Nagahama⁸

Abstract Multiple, gravity and piston cores were collected at four sites in the Chilean marginal area during the R/V MIRAI MR03-K04 cruise (leg.3, 15 October-2 November 2003). This cruise is a part of the BEAGLE (Blue Earth Global Ocean Experiment) program, a circumpolar cruise around the Southern Hemisphere, developed by JAMSTEC / POGO-IOCCG.

Here, we report the basic data on coring site locations and some geological data: visual core descriptions, color reflectance spectra, magnetic susceptibility, gamma ray attenuation density, and microfossil assemblage, which were determined on board the ship during the cruise.

Keywords: MIRAI, Chilean marginal area, Magellan Strait, sediment

1. Introduction

The Chilean marginal area is characterized by high productivity due to coastal upwelling and cold sea-surface water resulting from the Humboldt Current, which is the largest eastern boundary current in the global oceans. At subsurface water depths between 20° to 45°S, a zone of low oxygen concentration coincides with the Gunther Undercurrent; at latitudes south of 35°S, Antarctic Intermediate Water, which has a high oxygen and low nutrient and salinity, is present at depths of 500 - 800 m. As a result, the Chilean marginal area is a key area for the biogeochemical cycling of carbon in the global oceans, and has functioned in this role not only during the Holocene but also during the past glacial-interglacial periods. Despite its importance, few systematic surveys have addressed the temporal and spatial variation of biogeochemical processes in the area. The main goal of this research was to investigate historical changes in the biological pump, which transports carbon from the surface to the deep ocean, sea-surface water temperatures, and the ventilation rate of the intermediate water since the last interglacial.

Past variation and changes in the thermohaline circu-

lation and biogeochemical cycle recorded in marine sediments provide important information that can be used to predict future global climatic changes. Since a large part of Southern Hemisphere is occupied by ocean, the Southern Ocean significantly influences climatic change in the Southern Hemisphere.

This research addresses two themes: the carbon cycle and the phase lag or synchronization of the sea-surface environment between the Southern and Northern Hemispheres, both of which are extremely important topics in paleoceanography. For each theme, we propose and test a hypothesis. Based on our results, we describe past environmental changes throughout the Southern Hemisphere since the last deglacial period, and we also use our results to construct a paleoclimate model.

Carbon cycle

The vertical profile of pCO_2 in bubbles in the Vostok ice core shows that during the last glacial maximum (LGM), pCO_2 in the air was very low (220~200 ppm). The actual mechanism causing these low pCO_2 values has not been determined, but it is very possible that the pattern of ice distribution between land and ocean and

- 1 Japan Agency for Marine-Earth Science and Technology, 2-15 Natsushima-cho, Yokosuka 237-0061 Japan
- 2 Hokkaido University, Kita 10 Nishi 8, Kita-ku, Sapporo 060-0810 Japan
- 3 University of Concepción, COPAS, Casilla Correo 160-C, Barrio Universitario, Concepción, Chile
- 4 Nagoya University, Furo-cho, Chikusa-ku, Nagoya 464-8602 Japan
- 5 Kochi University, Center for Advanced Marine Core Research, 200 Monobeotsu, Nankoku 783-8502 Japan
- 6 Kyushu University, 6-10-1 Hakozaki, Higashi-ku, Fukuoka 812-8581 Japan
- 7 Marine Works Japan Ltd, 1-1-7, 2F Mutsuura, Kanazawa-ku, Yokohama 236-0031 Japan
- 8 Global Ocean Development Inc., 13-8 Kamiookanishi 1-chome, Konan-ku, Yokohama 233-0002 Japan

biogeochemical cycles in the ocean during the LGM were different from those during the Holocene. Several hypotheses have been proposed to explain the low pCO₂: (1) the carbon fixation ability of phytoplankton was higher in the LGM than in the Holocene because nutrient utilization was more efficient, or due to changes in phytoplankton assemblages; (2) primary production was higher in the LGM because of the presence of more dust-containing elements such as iron; or (3) less CO₂ was released from the surface of the Southern Ocean because of expansion of the sea-ice distribution.

We study sediment cores from the ocean bottom off Chile to estimate the degree to which sea-ice had expanded. If the sea-ice area in the Southern Ocean was larger during the LGM than during the Holocene, the polar front, which is found at $40^{\circ}\sim50^{\circ}\mathrm{S}$ in the modern South Pacific, would have migrated to a lower latitude. We collected three piston cores from between 30° and $60^{\circ}\mathrm{S}$ to estimate the paleo-sea-surface temperature by $\delta^{18}\mathrm{O}$ and alkenone methods and to determine the variation in the north–south migration of the polar front. Ice rafted debris (IRD) measurement is also important to understand the expansion of sea-ice distribution.

We also analyze opal and organic carbon content, biomarkers such as alkenones, and the stable isotopic ratios of carbon and nitrogen in bulk organic matter to investigate changes in primary production and the efficiency of nutrient utilization by phytoplankton from the terminal period of the last glacial episode to the Holocene. Furthermore, we measure the Cd/Ca ratio of planktonic and benthic foraminifera as a proxy for nutrient availability and estimate the difference in nutrient concentration between surface and deep waters to understand glacial—interglacial variations in the nutrient cycle in the Southern Ocean. In order to estimate wind intensity and changes in the dust supply through geological time, ratios of metal isotopes derived from dust (Rb:Sr, Sm:Nd, and Lu:Hf) are measured.

Climate linkages between the Northern and Southern Hemispheres

Seesawing bipolar climate changes on sub-Milankovitch to millennial timescales have been hypothesized by various researchers, based on climate reconstructions from both ice-sheet and deep-sea sediment records. However, no clear consensus on an interhemispheric climate linkage has yet been reached. Indeed, some researchers have argued for the synchronicity of interhemispheric climate change on the same timescales.

We analyze $\delta^{13}C$ and trace metals such as Mg and Cd in multiple species of planktonic foraminifera, the ^{14}C ages of planktonic and benthic foraminifera, and

alkenone SST with high time resolution in sediments from the region off Chile. These time-series data on ocean-surface environments make it possible to resolve sub-Milankovitch- to millennial-scale climate changes in the Southern Hemisphere. Although the detailed scientific results and discussion mentioned above will be reported elsewhere, in this report, we present only the primary results and basic data on the physical properties of the sediment cores, determined on board our research vessel.

2. Sampling locations

In all, four piston (PC), two gravity (GC), and four multiple (MC) cores were collected in the Chilean marginal area and Magellan Strait (Fig. 1 and Table 1). Cores PC-1 and MC-1 were collected at the southwestern of Valparaiso, Chile (Stn.1; 36°13'S, 73°41'W, water depth 1023 m). Cores PC-2, GC-1, and MC-2 were collected to the south of PC-1 (Stn.2; 39°59'S, 74°25'W, water depth 1064 m). Cores PC-3 and MC-3 were collected at the mouth of the Magellan Strait on

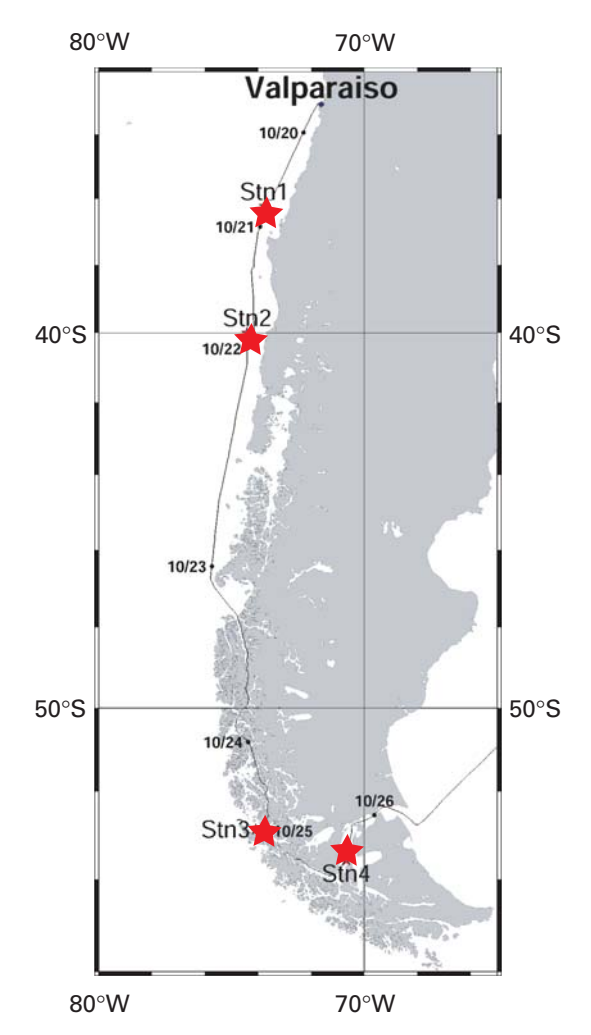


Figure 1: Location map of sediment cores collected at Chilean marginal area and Magellan Strait.

Stn	Core	Equipment	Latitude (S)	Longitude (W)	Water depth (m)	Cored length, including flow-in (cm)
1	PC-1	Piston corer	36°13.34'	73°41.00'	1023	766
1	MC-1	Multiple corer	36°13.00'	73°41.00'	1022	33
	PC-2	Piston corer	39°59.96'	74°25.16'	1064	791
2	MC-2	Multiple corer	39°59.98'	74°25.18'	1066	30
	GC-1	Gravity corer	39°59.98'	74°25.19'	1064	268
3	PC-3	Piston corer	52°52.00'	74°05.07'	562	964
	MC-3	Multiple corer	52°51.99'	74°05.02'	558	27
	PC-4	Piston corer	53°34.29'	70°40.49'	468	1851
4	MC-4	Multiple corer	53°34.26'	70°40.48'	469	44
	GC-2	Gravity corer	53°34.26'	70°40.56'	467	308

Table 1: Summary of sediment cores colleted during cruise MR03-K04 leg.3 in 2003

Table 2: Faunal groups observed in core catcher samples of piston and gravity cores during Leg.3 of MR03-K04. $a=>212 \mu m$, $b=150-212 \mu m$, ND=no data, 0=absent.

	PC-1		PC	C-2	PC-3		PC-4		GC-1		GC	2-2
Faunal Groups	a	b	a	b	a	b	a	b	a	b	a	b
Radiolaria	X	0	X	0	X				ND	0	0	
Sponge spicules		0		0		X			ND	0	0	
Bivalvia		0		0	X	X	X		ND	0	0	X
Pteropoda		0		0		X		X	ND	0	0	X
Dentalium,Scaphopoda		0		0	X		X		ND	0	0	
Ostracoda		0		0	X	X	X	X	ND	0	0	
Bryozoa		0		0		X			ND	0	0	
Spicules of Echinodermata	X	0		0					ND	0	0	
Fish remains	X	0		0					ND	0	0	X

the Pacific side (Stn.3; 52°52'S, 74°05'W, water depth 560 m). Cores PC-4, GC-2, and MC-4 were collected in the Magellan Strait (Stn.4; 53°34'S, 70°40'W, water depth 470 m).

3. Results

3.1 Visual core description

In general, the sediments at all sites are composed of homogeneous fine-grained hemipelagic sediments with various degrees bioturbation thourghout cores. The sediments, MC-1, PC-1, MC-2, PC-2 and GC-1 are dominated by clayey silt-silty clay with varying amount of diatom and nannofossil. These area consistent with the lithology of sites 1234 and 1233 of ODP leg.202). Sand content is highest for cores MC-3 and PC-3 in the Pacific inlet of Magellan Strait, while clay content is highest for cores MC-4, PC-4 and GC-2 in Magellan Strait. All cores have a wide variety of microfossils, being MC-3 and PC-3 the most diverse (Table 2). On

the other hands, MC-4, PC-4 and GC-2 have little amount of foraminifera and high content of continental components. These lighological and sedimentological features were summarized as graphic columns with short notes (Fig. 2).

3.2 Color reflectance

Color measurements of split cores are commonly used to acquire reflectance parameters, which indicate several characteristics of the sediments, such as lithology, oxidation rate, and concentrations of carbonates, organic matter, and certain inorganic compounds.

There are different systems for quantifying the color reflectance of soils and sediments, but the most common is the L*a*b* system, also referred to as the CIELAB system. This system can be visualized as a cylindrical coordinate system in which the axis of the cylinder is lightness (variable L*), ranging from 0% to 100% (black to white), and the radii are the chromatic

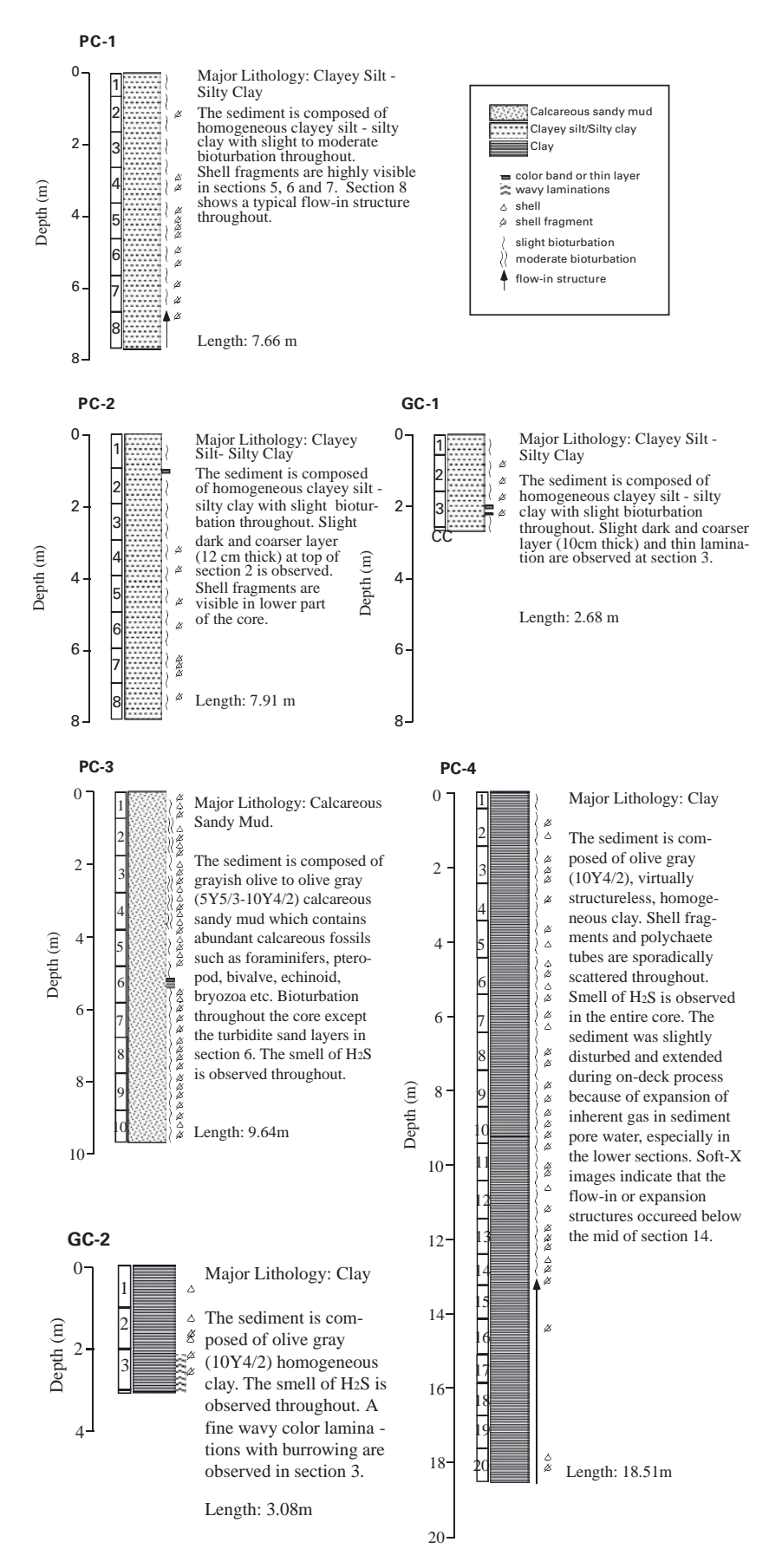


Figure 2: Lithological summary for sediment cores collected during MR03-K04 Leg.3. The major lithology is represented by graphic column. Numerals in the left side of graphic column indicate section numbers.

variables (a* and b*). Variable a* is the green (negative) to red (positive) axis, and variable b* is the blue (negative) to yellow (positive) axis.

A Minolta photospectrometer (CM-2002) was used in this leg to measure color reflectance parameters for wavelengths from 400 to 700 nm. This instrument measures the spectral reflectance of surface sediment with an 8-mm-diameter hole. To ensure accuracy, the CM-2002 was used with a double-beam feedback system, which monitored the illumination on the specimen at the time of measurement and automatically compensated for any changes in the intensity or spectral distribution of the light.

After the cores were split into two parts (A and B), each part was wrapped with a transparent polyethylene wrap (Saran wrap®; wraps made by other companies are not suitable, because the characteristics of wave lengths of colors transmitted through the wrap depend on the companies and Saran wrap® is the best for obtaining the color data). Part A was reserved for color measurements.

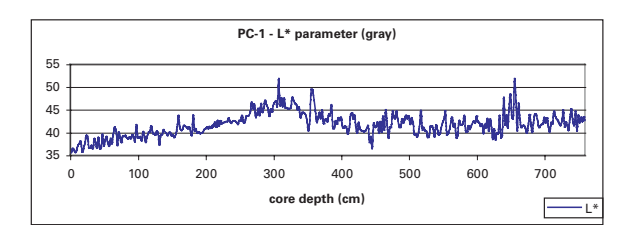
Before any measurement, the instrument was calibrated according to the manufacture's instructions. In addition, zero calibration can also compensate for ambient variations in temperature and humidity. White calibration was also performed before each measurement. The color was measured at 2-cm intervals in each core.

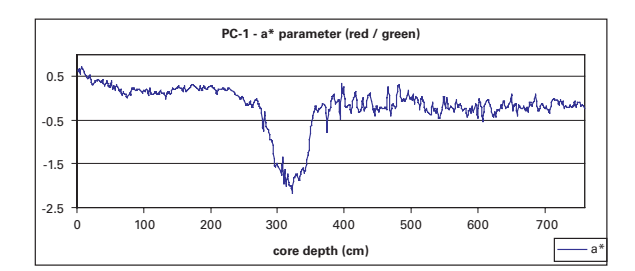
3.2.1 Color comparison between two cores collected at the same site

The data on color measurements are shown in Figs. 3–8. Since piston cores PC-2 and PC-4 were obtained at the same sites as gravity cores GC-1 and GC-2, respectively, the color parameters could be used to determine how much sediment was lost at the tops of the piston cores. This process produced good results when correlating between PC-2 and GC-1 (Fig. 9). By comparing the relative positions of color features, we were able to conclude that the top 1.36 m of core PC-2 had been lost. The comparison of cores PC-4 and GC-2 did not produce clear results because both PC-4 and GC-2 showed a chaotic distribution of stains of darker material all along the core, and also because of irregularities of the measurement surface of core PC-4.

3.2.2 L* parameter

The L* parameter (or gray level) is related to the carbonate content in the sediment. Although this relationship is not linear, it is possible to determine carbonate content semiquantitatively in this way. Thus, it is possible to observe the basic pattern of change in carbonate content from the L* parameter curves (Figs. 3-8). In





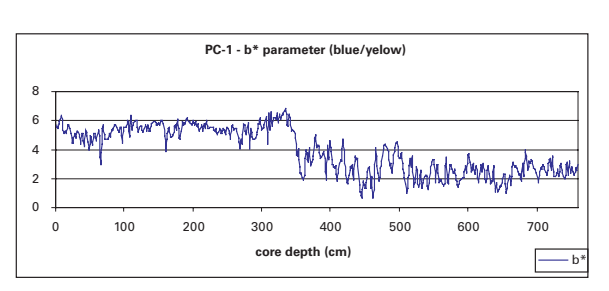
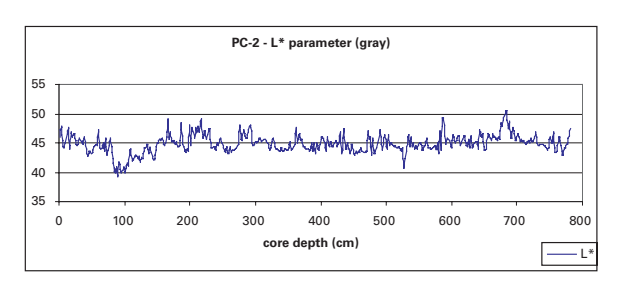
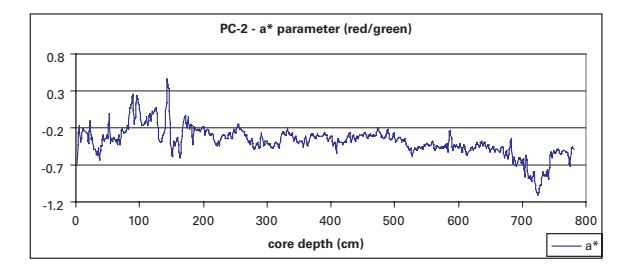


Figure 3: L*, a*, and b* parameters of PC-1





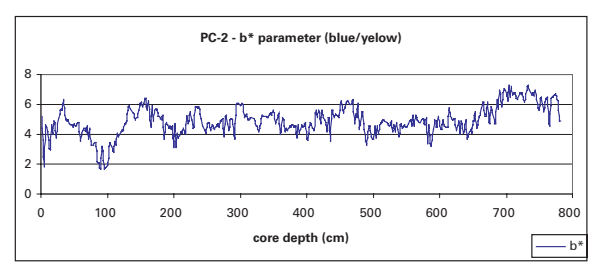
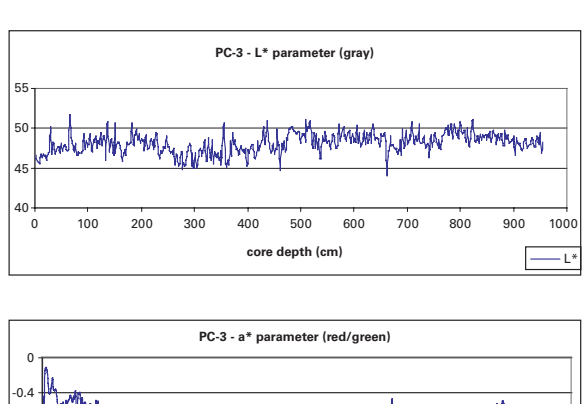
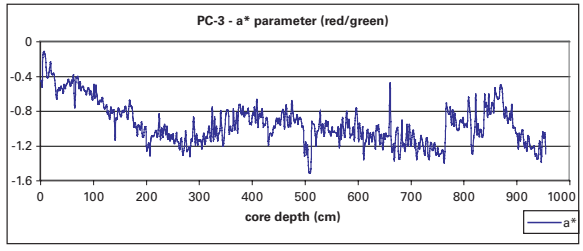


Figure 4: L*, a*, and b* parameters of PC-2





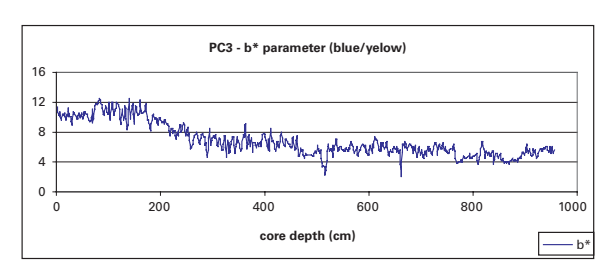
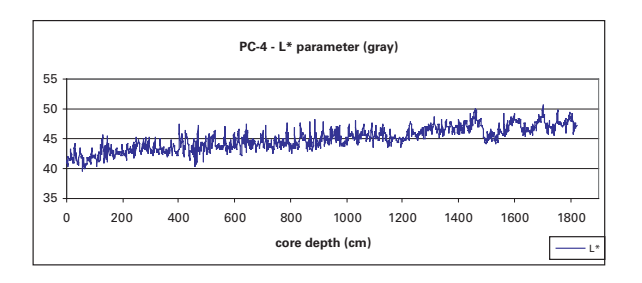
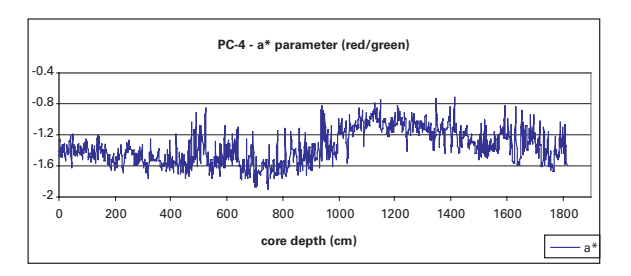


Figure 5: L*, a*, and b* parameters of PC-3





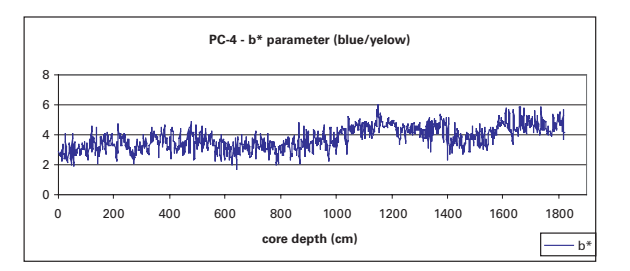
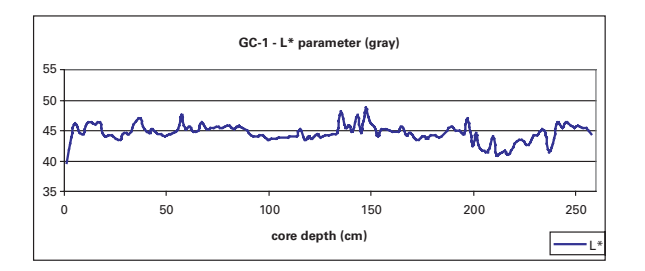
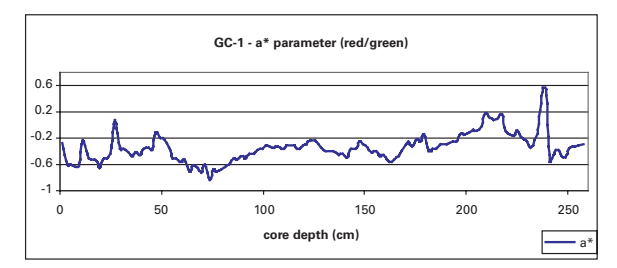


Figure 6: L*, a*, and b* parameters of PC-4





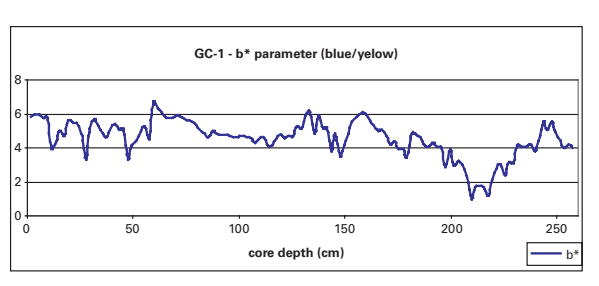
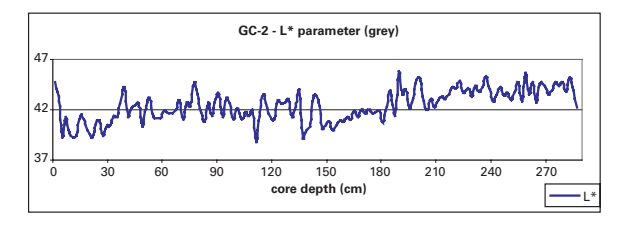
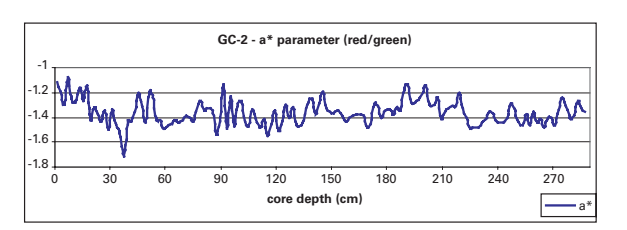


Figure 7: L*, a*, and b* parameters of GC-1





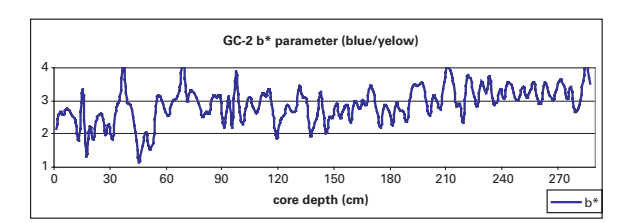


Figure 8: L*, a*, and b* parameters of GC-2

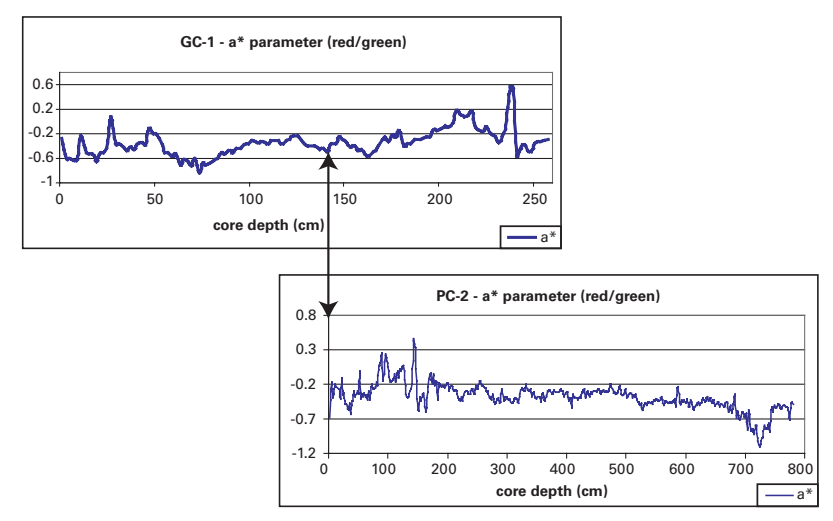


Figure 9: Parameter a*, showing how the top of core PC-2 correlates with core GC-1, thus indicating the amount of sediment lost from the piston core (~1.36 m).

PC-1, L* values increase from the top to 3 m depth, where $L^* = 53$, followed by a decrease from 3 to 4.5 m depth; L* then levels off at around 43, with one peak of 52 at about 6.5 m depth (Fig. 3). In PC-2 and PC-3, L* is relatively constant, with the exception of a dip in core PC-2 at 1 m depth (Figs. 4 and 5). In PC-4, L* tends to increase with depth (Fig. 6). The GC-1 showed relatively constant L* with depth. The GC-2 cores showed that L* values increase with depths (Fig. 8).

3.2.3 a* and b* parameters

Parameters a* and b* are not as clearly related to specific core features, nor do they show cyclic variations. They are, however, sensitive to clay mineralogy, nannofossil content, and so on. Peaks in the values of a* and b* may indicate changes in the lithology and in the concentrations of specific compounds, for example, the dramatic decrease in parameters a* (and b*) in PC-1 between 3 and 4 m depth (Fig. 3). However, significant lithological feature corresponding to this dramatic change in both parameters was not found in visual core description (Fig. 2). The parameters a* and b* can vary over just a few centimeters, as shown by narrow peaks on the graphs.

3.3 Multi-sensor core logging (MSCL)

Gamma-ray attenuation (GRA) and magnetic susceptibility (MS) were measured on whole-core sections with the onboard GEOTEK multi-sensor core logger (MSCL) to obtain primary data on wet bulk density, fractional porosity, and magnetic susceptibility. Wet bulk density and fractional porosity were calculated by assuming that only sediments and water were inside the core tube.

Medium-energy gamma rays (0.1-1 MeV) interact

with the material in the core mainly by Compton scattering. Because the elements of most rock-forming minerals have similar Compton mass attenuation coefficients, the measured electron density can easily be related to the material's bulk density. The ¹³⁷Ce source used transmits gamma rays at 660 KeV. A standard NaI scintillation detector was used in conjunction with a universal counter. Calibration of the GRA system for sediments and rocks assumes a two-phase system model, where the two phases are the minerals and the interstitial water. Aluminum has an attenuation coefficient similar to that of common minerals and is thus used as the mineral phase standard. The actual calibration instrument consists of a telescoping aluminum rod mounted in a section of the core liner and filled with distilled water. GRA was measured on the whole core at 2-cm intervals; counting was performed for 10 s. GRA data can be used to determine wet bulk density and fractional porosity when the core thickness is constant (thicknesses: multiple core, 74 mm; piston core, 80 mm; gravity core, 120 mm).

MS was measured using a Bartington MS2C system within the MSCL. The main unit is the widely used, versatile MS2C susceptometer, which is capable of rapid measurements with a number of sensors. The unit has a measuring range of 1×10^{-5} to 9999×10^{-5} (SI, volume specific). The loop sensor for piston and multiple cores has an internal diameter of 100 mm. It operates at a frequency of 0.565 kHz and an alternating field (AF) intensity of 80 A/m (= 0.1 mT). MS was measured on the whole core at 2-cm intervals, with each measurement being 1 s long. MS data are a relative proxy indicator for changes in magnetic particulate composition, which can be linked to paleoclimatic changes that affect depositional processes.

3.3.1 General interpretation of MSCL data

From the top to a few tens of centimeters of depth, gamma density generally increased greatly and fractional porosity decreased drastically because of the rapid decrease in water content. Raw magnetic susceptibility and gamma ray attenuation data are generally inversely correlated; thus, volumetric magnetic susceptibility and gamma bulk density are directly correlated. These relationships imply that high bulk density (low gamma ray attenuation) intervals are associated with a high magnetic material content.

3.3.2 PC-1 and MC-1 (Fig. 10)

The fractional porosity, gamma density, and magnetic susceptibility data could not be correlated among MC-1, and the top of the piston core, implying that a few tens of centimeters were lost from the top of the piston core. Magnetic susceptibility gradually decreased from 20 cm to 1 m depth. Very low magnetic susceptibility values were obtained from 2.5 to 3.5 m depth. However, no core feature noted in the visual core description corresponded to the low magnetic susceptibility interval.

3.3.3 PC-2, GC-1, and MC-2 (Figs 11 and 12)

Data from sections 1 and 2 of PC-2 and section 1 of GC-1 were not available because there were many tiny gas-filled holes in the sediment. The visual core description and color parameters showed that the top 1.6 m of

the piston core was lost because of the impact of the corer with the seafloor. However, a similar loss of piston core MSCL data was not detected by the comparison between PC-2 and GC-1. The profiles of magnetic susceptibility, fractional porosity, and gamma bulk density were constant throughout the entire core except for two spikes at depths of 3.8 and 5.8 m.

3.3.4 PC-3 and MC-3 (Fig. 13)

Peaks and troughs of magnetic susceptibility were well correlated with those of gamma density. The profile patterns imply that high bulk density (low gamma ray attenuation) intervals are associated with a high magnetic material content. Although no large spikes of magnetic susceptibility or gamma density were found in the top 5 m of the profiles, the frequency and amplitude of changes in magnetic susceptibility and gamma density were high at depths below 5 m.

3.3.5 PC-4 and MC-4 (Fig. 14)

Peaks and troughs of magnetic susceptibility showed good correlation with those of gamma density. The profile patterns imply that high bulk density (low gamma ray attenuation) intervals are associated with a high magnetic material content. Magnetic susceptibility and gamma density were constant in the top 4 m, but the frequency and amplitude of changes in magnetic susceptibility and gamma density were high at depths below 4 m.

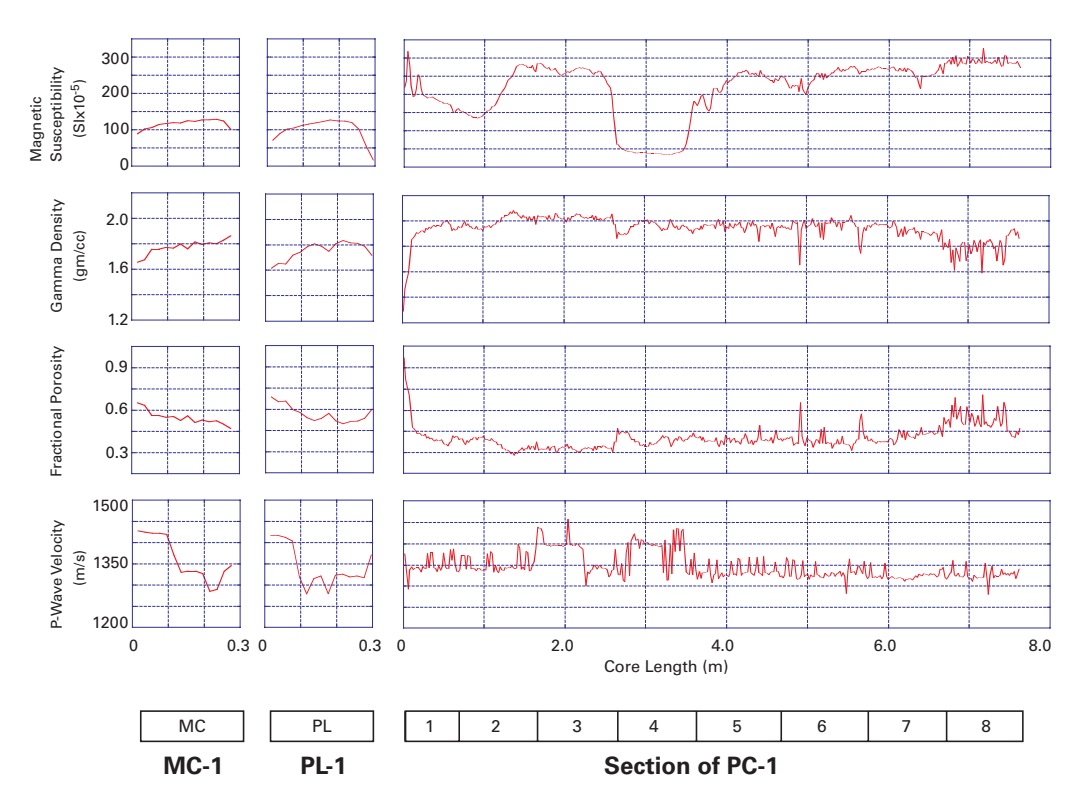


Figure 10: MSCL data of PC-1, PL-1 and MC-1

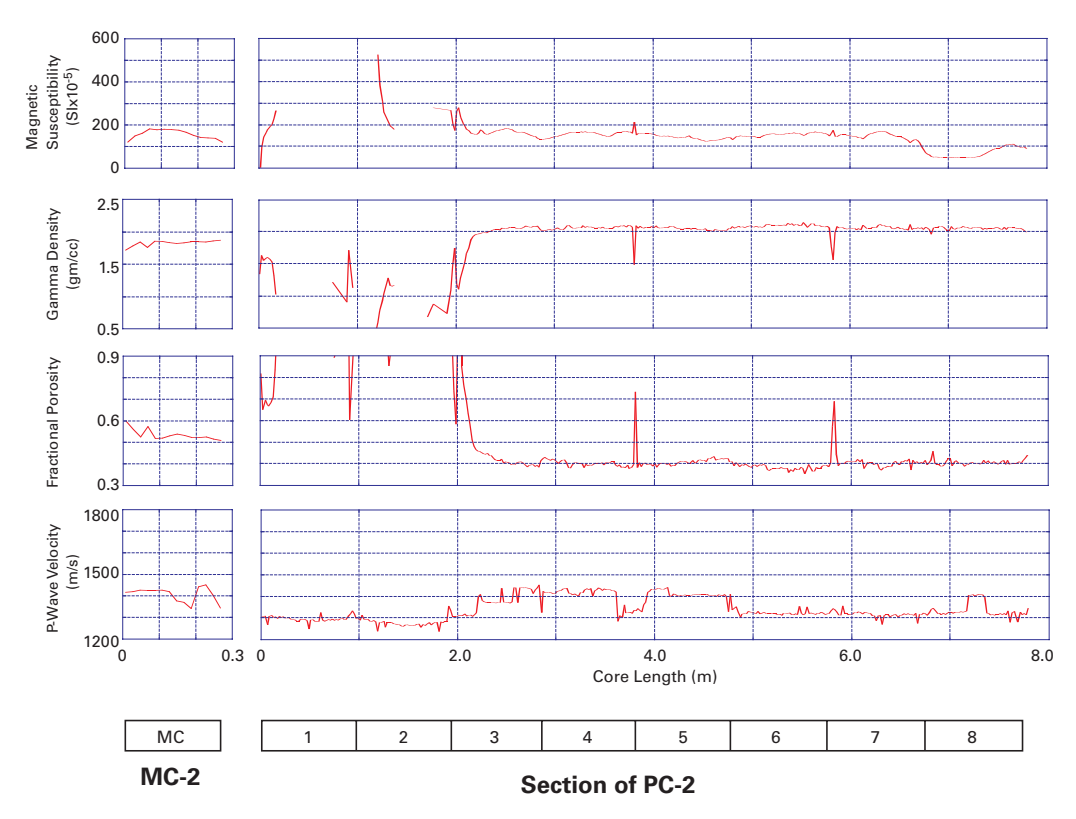


Figure 11: MSCL data of PC-2 and MC-2

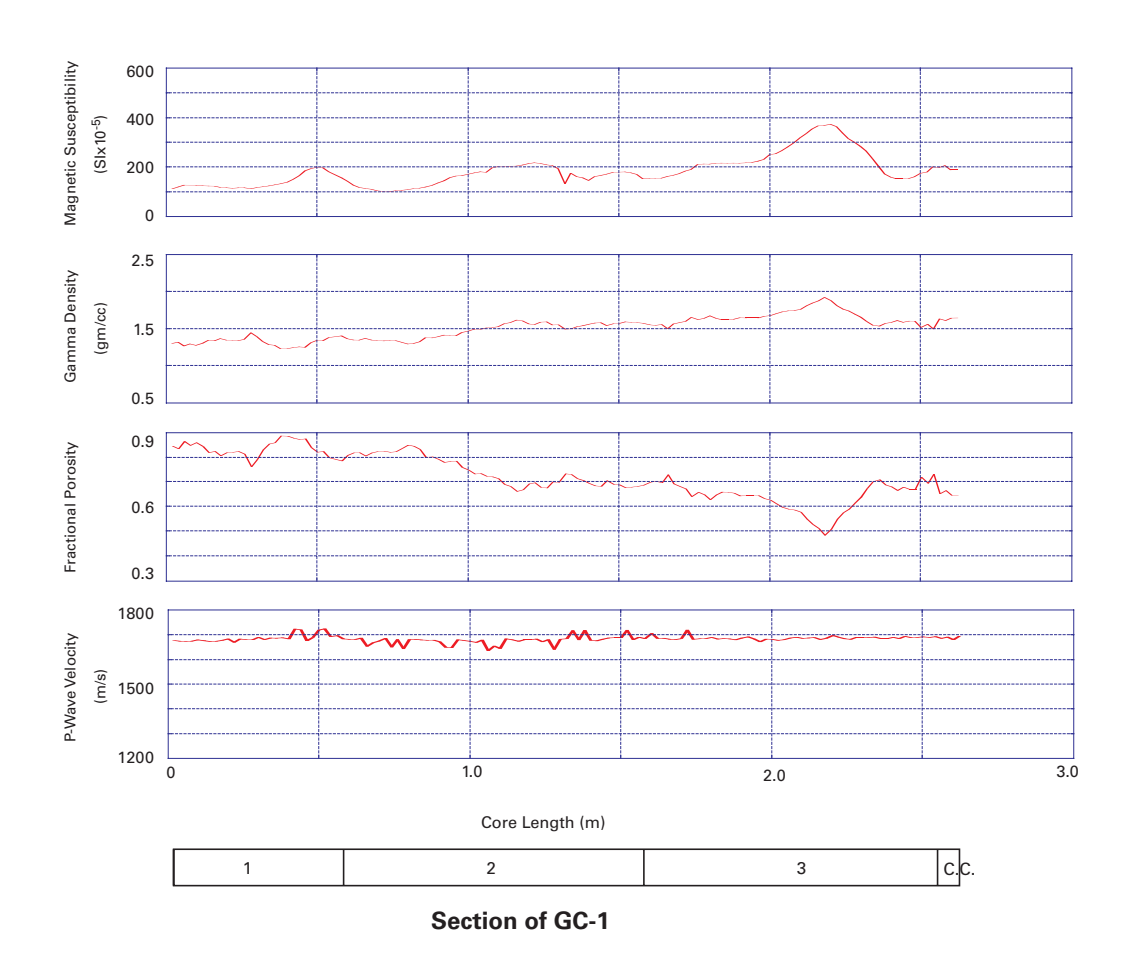


Figure 12: MSCL data of GC-1

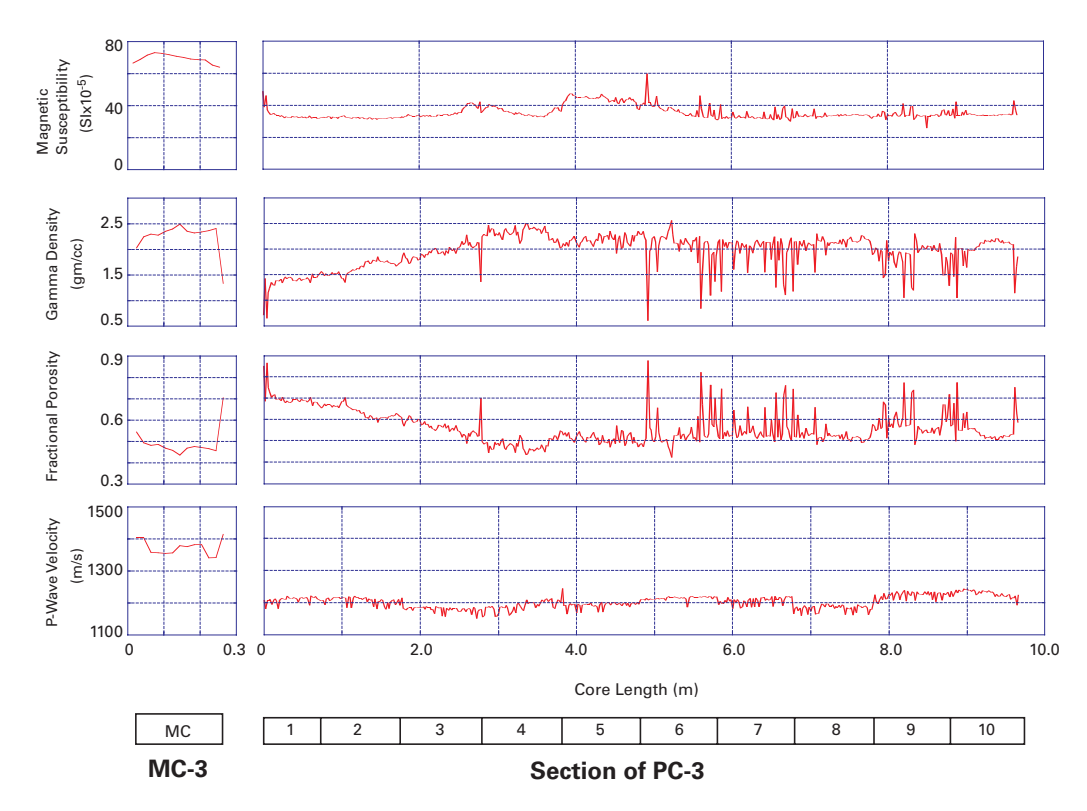


Figure 13: MSCL data of PC-3 and MC-3

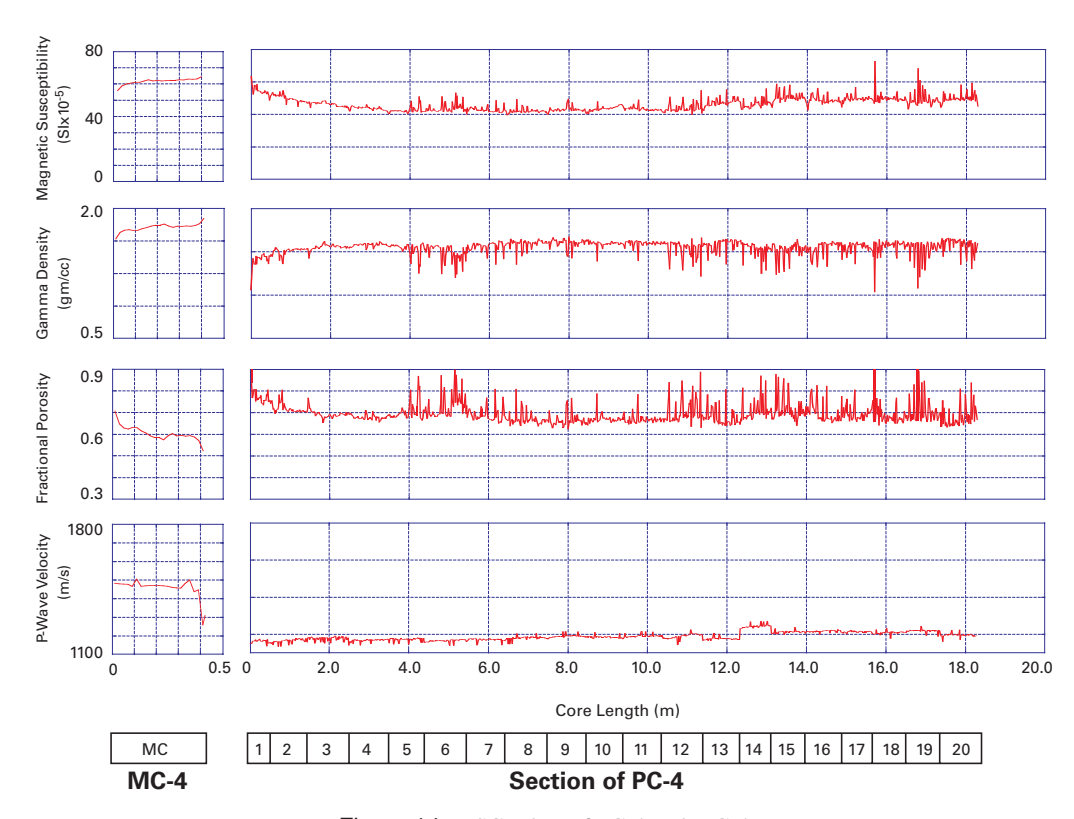


Figure 14: MSCL data of PC-4 and MC-4

3.4 Microfossils

The sediment in core catchers of piston and gravity cores was divided into 3 samples; one for foraminifera, the second one for radiolarians and the third one was kept as archive. Samples for foraminifera were analysed for general microfossil content (Table 2) and preliminary detailed foraminifera analysis (Tables 3 and 4). Samples were sieved through three different sieves and divided into three fractions (>212, 150-212 and 63-150 µm sieves), dried in an oven at 50°C and once dried kept in vials.

The results presented here refer to the two bigger fractions. These were observed under an Olympus stere-oscope. Relative abundances are based on a total of >200 individuals per sample. A short characterization of the types of microfossils found in the cores is given below, and details are shown in Tables 2-4.

3.4.1 PC-1

Radiolaria, test of Echinodermata and Pisces were observed in the 212 μm fraction. The highest concentrations of planktic and benthic foraminifera were found in this piston core among the four sites. The dominant species are *Uvigerina peregrina* (*U. peregrina*) (benthics) and *Globigerina bulloides* (*G. bulloides*) (planktics). *Neogloboquadrina pachyderma* (*N. pachyderma*) (sin.) accompanies these species in the 150-212 μm fraction.

3.4.2 PC-2

Only Radiolarians were observed as accompanying the foraminiferal assemblages. The concentration of benthic foraminifera is relatively low while planktics are abundant. The benthic assemblage is dominated by *U. peregrina.* Planktic foraminiferal assemblage is typical of a transitional fauna and is characterized by *G. bulloides, Globorotalia inflata* (*G. inflata*) and *N. pachyderma* (dex.). In the 150-212 μm fraction, *N. pachyderma* (sin.) and (dex) are present in equal proportions.

3.4.3 GC-1

The same pattern as in PC-2 is seen in this core. The characteristic species of this transitional area are G. bulloides, G. inflata in the >212 μ m fraction and N. pachyderma (sin.) and (dex.) in the intermediate fraction. The dominant benthic species are U. peregrina and Praeglobobulimina pyrula.

3.4.4 PC-3

This site is the most diverse: Radiolaria, Bivalvia, Pteropoda, Scaphopoda, Bryozoa, Porifera and Ostracoda are present. After sieving, a lot of sediment remained in the 63-150 µm fraction. Qualitative analysis revealed the presence of: Pteropoda, sponge spicules, Ostracoda and tests of Echinodermata. As for foraminifera, *N. pachyderma* (sin.) and benthic foraminifera like *Tetronphalus bulloides* (*T. bulloides*), *Cibicides elmaensis* (*C. elmaensis*), *Patellina corrugata*, *Cassidulina delicata* (*C. delicata*) and the genera *Bolivina*, *Spirillina* and *Elphidium* were observed.

The benthic foraminiferal assemblage is very diverse in the >212 μ m with 18 species. *Quinqueloculina seminula* (*Q. seminula*) and *Florilus grateloupi* (*F. grateloupi*), which are typical shelf species dominate. The important species in the 150-212 μ m fraction are *C. delicata*, *C. elmaensis*, *F. grateloupi*, *Q. seminula* and *T. bulloides*. The diversity of planktic foraminifera is

Table 3: Planktic foraminifera observed in	core catcher samples of piston ar	d gravity cores during Leg 3 of MR03-
K04. $a = >212 \mu m$, $b = 150-212 \mu r$	n.	

	PC-1		PC	-2	PC-3		PC-4		GC-1		GC-2	
Planktic Foraminifera	a	b	a	b	a	b	a	b	a	b	a	b
Globigerina bulloides	266	32	82	12	104	67	1		103	14	1	12
Globigerinita glutinata	9				2		2	4	2	22		4
Globorotalia crassaformis			2									
Globorotalia inflata	35	10	72	52					53			
Globorotalia scitula	1	8		4						2		
Gl.truncatulinoides	3				1							
Globorotaloides hexagonus			2									
N. pachyderma (sin.)	7	96		64	2	26			1	88		
N. pachyderma (dex.)		12	30	76	4	27			6	90		
Orbulina universa		2	8						4			
Turborotalia quinqueloba										2		
Total	281	160	196	208	112	121	3	4	169	216	1	16

Table 4: Benthic foraminifera observed in core catcher samples of piston and gravity cores during Leg 3 of MR03-K04. $a = >212 \, \mu m$, $b = 150-212 \, \mu m$.

	PC	:-1	PC	-2	PC	!-3	PC	C-4	GC-1		GC-2	
Benthic Foraminifera	a	b	a	b	a	b	a	b	a	b	a	b
Astrononion sp.				4	2		1	24				44
Bulimina inflata	2	40		12		1				18		
Bucella peruvianus					2		1	18				8
Cassidulina laevigata	2	12		12		5		4		4		4
Cassidulina delicata						15	8	92			25	64
Chillostomella sp.									1			
Cibicides elmaensis	1		2		14	12	20	102			34	60
Cibicides ornatus	13	2	2						4			
Cibicides variabilis		2			2		2	2	-			4
Cibicides wuellerstorf	9											
Cibicides		2										
Dentalina elegans	1	2										
"Elphidium"	1	26										
Ehrembergina pupa									2			
Fissurina sp.	1		2						3	1		
Florilus grateloupi	1				32	11		10		1	17	20
Fursenkoina		2			32	11		10		3	17	
Globobulimina	1											
Guttulina comunnis	1		2						2			
Gyroidina soldani									6			
Hoeglundina elegans			2						7			
Lagena aspera						1		2	/			
Lagena sp.					5	1	1	4			1	4
Lenticulina australis					2		1	2			1	4
Martinotiella comunnis	1										1	
Melonis pompilius	1								2			
Mililinella labiosa					1	1			3			
					1	1	4	2				
Nonionella turgida Nonionella		6	2				4					
Oridorsalis umbonatus	-		2									
	9					4						
Patellina corrugata	20	1.7		4	0	4			15			4
Praeglobobulimina pyrula	29	15	6	4	8	1	1		17	5	7	
Pullenia bulloides	2											
Pullenia subcarinata					5			2	1	1	1	
Pyrgo nasuta					1							
Pyrgo notalaria					1							
Pyrgo ringens							8		4		47	
Pyrgo sp.	1	2	2					2				8
Quinqueloculina seminula	-				47	30	25	12			70	24
Robertina arctica							1					
Spirillina sp.					1	9						
Tetromphalus bulloides					1	20		4		4		
Textularia gramen					1							
Trifarina carinata				4	8							
Triloculina			2							1		
Uvigerina peregrina	138	62	34	12			38	14	25	13	31	4
Virgulinella sp.		8										
Indeterminated					1	2					1	
Total	210	181	56	48	134	112	110	296	75	50	235	248

low with one dominant species in the $>212 \mu m$ fraction, *G. bulloides*. This species together with *N. pachyderma* (dex.) and (sin.) dominant the 150- 212 μm fraction, and the proportion of the two kinds of *N. pachyderma* is basically the same.

3.4.5 PC-4

Dentalium, Bivalvia, Ostracoda and Pteropoda are present. This site showed the lowest concentrations and diversity of foraminifera among the four sites. Planktic foraminifera are almost absent. The most important species of benthic foraminifera in both fractions are C. *elmaensis*, *Q. seminula* and *U. peregrina*.

3.4.6 GC-2

The sample shows fish remains, Pteropoda and Bivalvia. As with PC-4, the concentration and diversity of foraminifera was low. The entire >212 µm fraction was analysed. Planktic foraminifera are practically absent. The most important benthic species are *Q. seminula* accompanied by other species as *C. delicata*, *C. elmaensis*, *F. grateloupi*, *Pyrgo ringens* and *U. peregrina*.

4. Summary

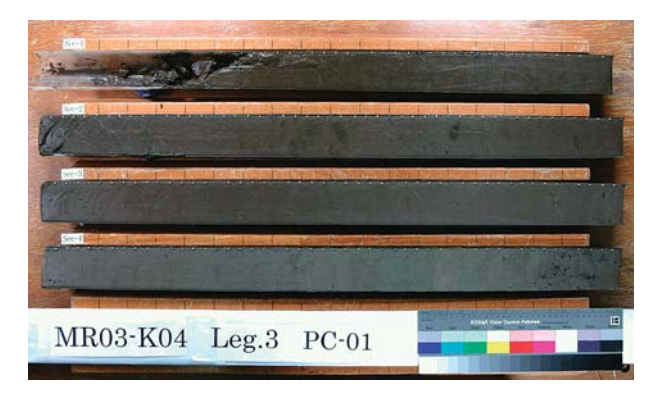
- (1) Four PC, two GC and four MC cores were collected in this MR03-K04 cruise. Three stations were located in the Chilean marginal area and another was located in the Magellan Strait. All cores are composed of homogeneous fine-grained hemipelagic sediments.
- (2) According to the visual core description and L* data, the carbonate content was the highest for sediment collected at St. 3. In addition, microfossil analysis showed that sediment at St.3 was the most diverse of fossil assemblage.
- (3) Magnetic susceptibility data showed that the sediment collected at Sts. 1 and 2 had higher values of one order rather than those at Sts. 3 and 4. In particular, the sediment at St. 4 showed very low value of magnetic susceptibility (~80). These implies that the organic material content might relate to the magnetic susceptibility data and the much amount organic materials originated from lithogenic would contribute to such low magnetic susceptibility.

References

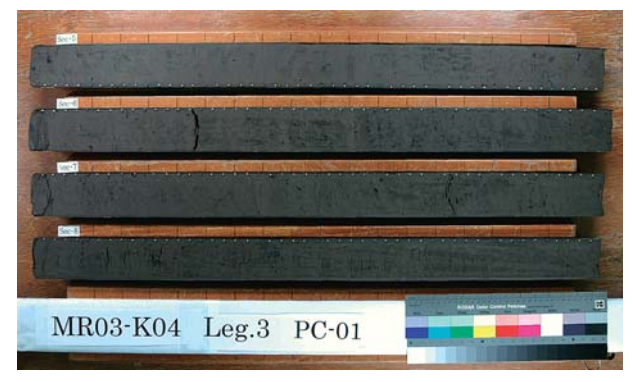
 A. C. Mix, et al., "Proc. ODP, Init. Reports" [CD-ROM]. Available from: Ocean Drilling Program, Texas A&M University, College Station TX 77845-9547, USA (2003).

(Received August 2, 2005)

Appendix



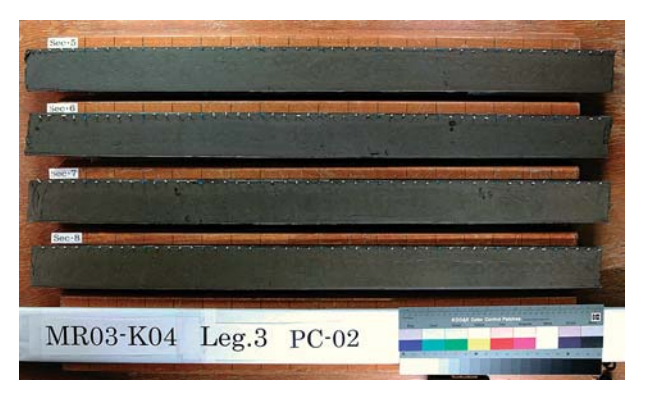
PC-01 Sec.1-4



PC-01 Sec.5-8



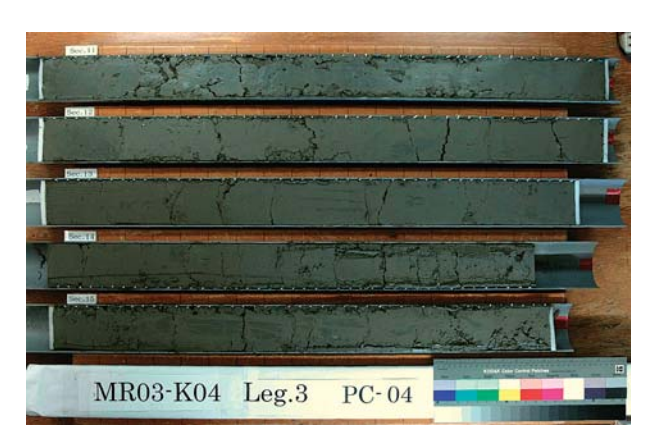
PC-02 Sec.1-4



PC-02 Sec.5-8



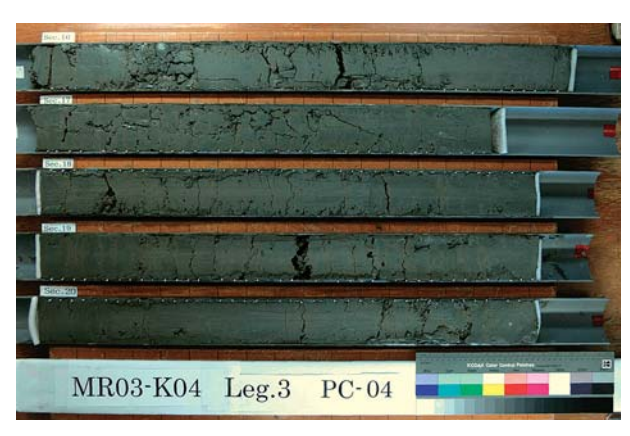
PC-03 Sec.1-5



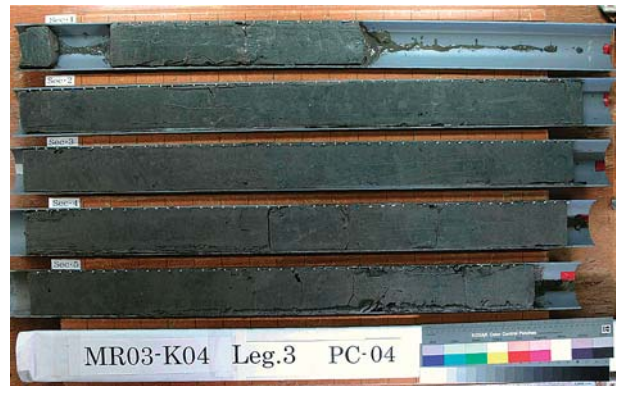
PC-04 Sec.11-15



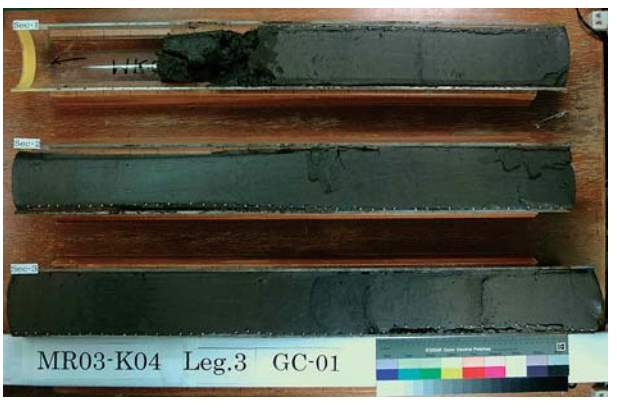
PC-03 Sec.6-10



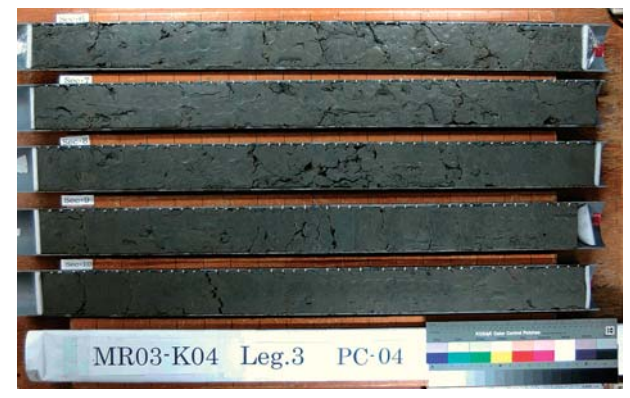
PC-04 Sec.16-20



PC-04 Sec.1-5



GC-01 Sec.1-3



PC-04 Sec.6-10



GC-01 C.C.



GC-02 Sec.1-3



GC-02 C.C.



MC-01 HAND-1



MC-02 HAND-1



MC-03 HAND-8



MC-04 HAND-1



PL (pilot core) -01 HAND-1